12th International Conference on Applications of Statistics and Probability in Civil Engineering, ICASP12
Vancouver, Canada, July 12-15, 2015

Reducing Wind Turbine Load Simulation Uncertainties by Means of a Constrained Gaussian Turbulence Field

Nikolay Dimitrov
Research Scientist, Dept. of Wind Energy, Technical University of Denmark, Denmark

Boyan Lazarov
Senior Scientist, Dept. of Mechanical Engineering, Technical University of Denmark, Denmark

ABSTRACT: We demonstrate a method for incorporating wind measurements from multiple-point scanning lidars into the turbulence fields serving as input to wind turbine load simulations. The measurement values are included in the analysis by applying constraints to randomly generated turbulence fields. A numerical study shows the application of the constrained turbulence method to load simulations on a 10MW wind turbine model, using two example lidar patterns – a 5-point pattern forming a square with a central point, and a circular one. Based on the results of this study, we assess the influence of applying the proposed method on the statistical uncertainty in wind turbine extreme and fatigue loads.

1. INTRODUCTION

Mechanical loads on wind turbines are to a large extent driven by the variations in the stochastic wind field entering the turbine rotor plane. Due to the large volumes involved and the complexity of the turbulent flow, it is currently not possible to characterize the incoming wind field entirely by measurements. Hence, in numerical load simulations, the turbulent wind is usually modelled as a random 3-dimensional Gaussian field with spectral properties defined by a turbulence model, e.g. the Veers (1988) and Mann (1994) models. For the purpose of load verification, the statistical properties (mean and variance) of the generated numerical field are defined to match the statistical properties of time series obtained by measurements at one or few points in front of the turbine rotor. Due to the stochastic nature of the problem, the instantaneous values of a generated field realization will not match the true values experienced by the turbine. As a result, the outcomes of a well-performing numerical load analysis will match the measured load values on average, however there will be a significant sample-to-sample variation due to the statistical uncertainty. Thus a significant number of observations and simulations are required for successful load verification of wind turbine prototypes.

Recent developments in the remote sensing technology have made it possible to simultaneously measure wind velocities in multiple points in a predefined pattern, by means of multiple-beam lidars and scanning lidars. Although not being able to characterize the entire turbulent wind field, the multi-point measurement technology can provide significantly more information for the incoming wind compared to measurements in a single point as provided by e.g., cup or sonic anemometers. As a result it is expected that incorporating multi-point lidar measurements in load simulations will reduce the sample-to-sample uncertainty of numerical load simulations with respect to observed wind turbine loads. In the present paper we explore this hypothesis by a numerical study which assesses the possible effect of including wind velocity values measured by multi-point lidar in the turbulence field used for aeroelastic load simulations. Lidar measurements are simulated by the implementation of constrained Gaussian

turbulence field, where each instantaneous measured value is treated as a constraint. In the following sections we describe the process of generating a constrained turbulence field, and assess the significance of using a constrained field on the load uncertainty.

2. GENERATING CONSTRAINED TURBULENCE FIELDS

2.1. Constrained Gaussian fields

The algorithm we use for applying constraints on a Gaussian field requires the use of a source, unconstrained realization of the random field, and defines a modified field which represents the most likely realization satisfying all constraints while retaining the crossing rates specific to the source field. Below, we give a short overview of the method, which is described in more details in Hoffman & Ribak (1991) and Nielsen et al. (2004).

Consider a zero-mean, homogeneous and isotropic Gaussian random field $g(\boldsymbol{r})$ which is defined by its power spectrum $S_r(\boldsymbol{k})$, and is subjected to a set of constraints $\Gamma = \{C_i(\boldsymbol{r})|_{r_i} = c_i,\ i = 1, \dots, M\}$. The conditional probability distribution of the field $g(\boldsymbol{r})$ is given by

$$P[g(\boldsymbol{r})|\Gamma] = \frac{P[g(\boldsymbol{r}), \Gamma]}{P[\Gamma]} \qquad (1)$$

where $P[.]$ is the multivariate Normal (Gaussian) distribution. $P[g(\boldsymbol{r})|\Gamma]$ is a shifted Gaussian field with ensemble mean of

$$\bar{g}(\boldsymbol{r}) = \langle g(\boldsymbol{r})|\Gamma\rangle = \boldsymbol{\zeta}(\boldsymbol{r})\mathbf{Z}^{-1}\boldsymbol{C} \qquad (2)$$

where $\langle . \rangle$ denotes ensemble averaging, $\boldsymbol{\zeta}(\boldsymbol{r}) = [\langle g(\boldsymbol{r})C_1\rangle, \langle g(\boldsymbol{r})C_2\rangle, \dots, \langle g(\boldsymbol{r})C_M\rangle]$ is a vector of the cross-correlations between the field and the constraints, $\mathbf{Z}$ is the correlation matrix of the constraints set, $\mathrm{Z}_{ij} = \langle C_i C_j\rangle,\ i = 1 \dots M, j = 1 \dots M$, and $\boldsymbol{C} = [C_1, C_2, \dots, C_M]^T$ is a vector with the constraint values. For a given realization of the field, the deviation between the field and the mean is denoted as the residual field, $\varepsilon_g(\boldsymbol{r}) = g(\boldsymbol{r}) - \bar{g}(\boldsymbol{r})$. The variance of the residual field is given by

$$\langle \varepsilon_g^2(\boldsymbol{r})|\Gamma\rangle = \sigma^2 - \boldsymbol{\zeta}(\boldsymbol{r})\mathbf{Z}^{-1}\boldsymbol{\zeta}(\boldsymbol{r})^T \qquad (3)$$

Any constrained realization can be written as a sum of the mean constrained field $\bar{g}(\boldsymbol{r}) = \langle g(\boldsymbol{r})|\Gamma\rangle$ and the random residual field $\varepsilon_g(\boldsymbol{r})$. As Equation (3) shows, the variance of the residual field is independent of the constraint values, which means that it is possible to construct a constrained realization of a Gaussian field using a theoretical estimate of the mean conditional (constrained) field, and a random residual field. Using this property, a constrained realization is obtained using the following steps: 1) generate an unconstrained, random realization $\tilde{g}(\boldsymbol{r})$; 2) find the values of the unconstrained realization corresponding to the constraints (i.e. at the same location and contemporaneous with the constraints), $\tilde{g}_c(\boldsymbol{r}) = \tilde{g}(\boldsymbol{r} = \boldsymbol{r}(c_i)),\ i = 1 \dots M$; 3) calculate the mean of the realization; 4) evaluate the residual of the realization; and 5) combine the residual with the constrained mean. Based on this algorithm, the constrained field is expressed as

$$g(\boldsymbol{r}) = \tilde{g}(\boldsymbol{r}) + \boldsymbol{\zeta}(\boldsymbol{r})\mathbf{Z}^{-1}[\boldsymbol{C} - \tilde{g}_c(\boldsymbol{r})] \qquad (4)$$

2.2. Turbulence boxes with constraints modelling lidar measurement patterns

The wind field which serves as input to aeroelastic wind turbine load simulations is typically defined in terms of a random, 3-dimensional turbulence field discretized on a rectangular grid (Figure 2). This discretized random field is called a turbulence box. The wind direction is considered coincident with the longest dimension of the turbulence box (here given as the x-coordinate), while the y- and z-coordinates cover the dimensions of the rotor plane. During a dynamic load simulation, the field over the wind turbine rotor is defined by a cross section of the turbulence box in the y-z plane, with the x-coordinate of the cross section representing a time axis. As the load simulations are usually carried out for a fixed time period, the mapping between the time and physical coordinates (meters) on the x-axis will depend on the required average wind speed. The

properties of the turbulence box are defined based on a spectral turbulence model, e.g., the Mann model (1994), and the values are generated using Fourier simulation. For the purpose of efficient utilization of the fast Fourier transform, the grid sizes are usually defined in powers of two, and in the present study we use turbulence boxes with grid size of $8192 \times 32 \times 32$ (x, y, z).

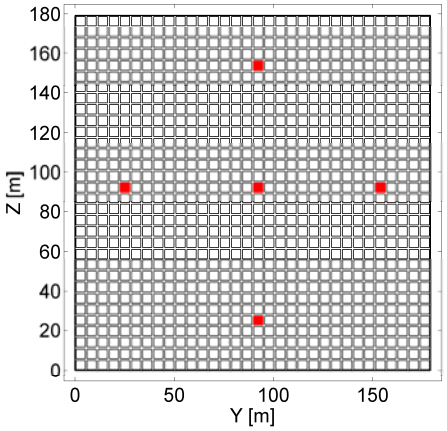

Figure 1: Constraint pattern representing measurements from a multiple-beam lidar with 5 beams, shown in the Y-Z plane of a turbulence box grid.

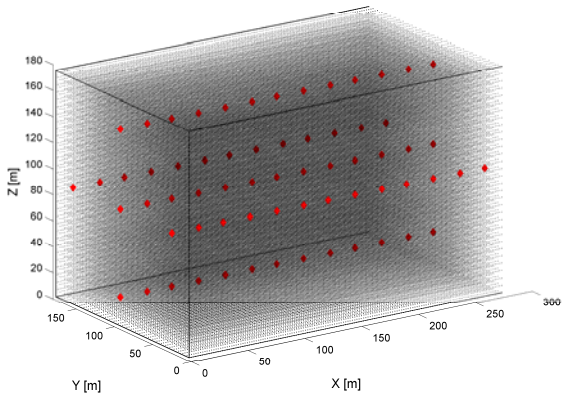

Figure 2: Three-dimensional view of a turbulence box including constraints with pattern representing measurement from a multiple-beam lidar with 5 beams.

For the purpose of assessing the possible effect of incorporating lidar measurements of wind velocity in wind turbine load simulations, we define two constraint patterns which, when applied to the turbulence boxes, mimic the measurement pattern of two types of multiple-point scanning lidars:

1) A multiple-beam lidar with 5 beams, with a center beam pointing forward and four beams pointing above, below, to the left and to the right of the center beam. The angle between each of the side beams and the central beam equals $15°$. All beams measure simultaneously in a vertical plane with measurement frequency of 1Hz. The pattern is shown on Figures 1 and 2.
2) A lidar with a single, rotating beam with $15°$ cone angle, rotating with angular velocity of 2.3 rad/s and measurement frequency of 11.72Hz. One revolution lasts 2.73 seconds and consists of 32 measurement points. The sampling frequency is chosen in a way that the time step between two successive lidar samples equals the step size in the turbulence box x-axis for a turbulence box with total duration of 700s. The resulting spiral-shaped pattern is shown on Figures 3 and 4.

The size of the two scanning patterns is chosen such that the measurement point locations approximately correspond to a radial distance of 2/3 blade lengths from the wind turbine hub. This is typically the radial position with the maximum aerodynamic forces acting on the blade, and we consider it as the most relevant placing in the case when only one radial distance can be measured. The mapping between the coordinates of the scanning points and the coordinates of the turbulence box grid is done by nearest-neighbor interpolation.

At each grid location, the instantaneous wind velocity is regarded as a 3-component vector $[u, v, w]$, where the three components quantify the wind velocity projection on the x, y and z axes respectively. The u, v and w

components are usually considered individually where each component is stored in a separate turbulence box. Applying constraints to all three components simultaneously will require a prohibitively large correlation matrix and will increase the computational expenses significantly. In the present study, we only apply constraints on the u component as it is the one with largest variance and most significant contribution to loads on wind turbines.

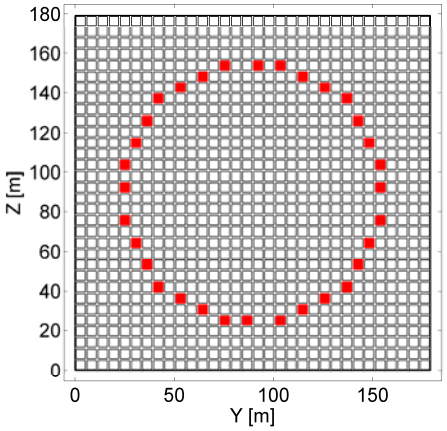

Figure 3: Constraint pattern representing measurements from a rotating-beam lidar with 32 measurement points per revolution, shown in the Y-Z plane of a turbulence box grid.

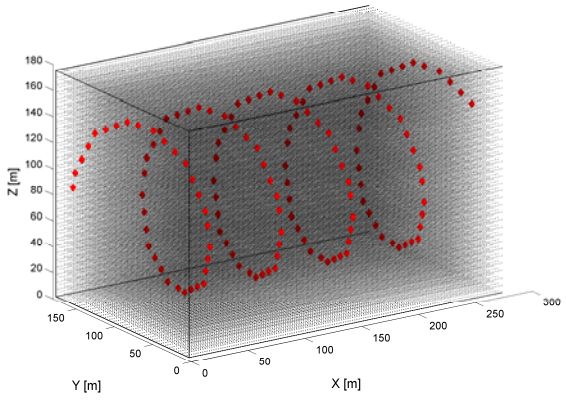

Figure 4: Three-dimensional view of a turbulence box including constraints with pattern representing measurement from a rotating-beam lidar with 32 measurement points per revolution.

2.3. Spectral properties of turbulence

The statistical properties of the turbulence fields used in the present study are based on Mann's uniform shear spectral model (Mann, 1994). The Mann model uses an isotropic von Karman turbulence energy spectrum, which is modified to account for the shear deformation and dissipation of the turbulence eddies caused by interaction with the ground surface. The model has three parameters: Γ is a non-dimensional number parameterizing the eddy lifetime; L is a length scale describing the size of the most energy-containing eddies; $\alpha\epsilon^{2/3}$ is a measure of the energy dissipation. The spectral properties are defined in terms of a spectral velocity tensor, $\Phi_{ij}(\boldsymbol{k})$, which is a function of the three parameters Γ, L, and $\alpha\epsilon^{2/3}$, and the wave numbers in three dimensions, $\boldsymbol{k} = [k_1, k_2, k_3]$. The cross-spectra $\chi_{ij}, i = 1 \dots 3, j = 1 \dots 3$, are obtained by integrating the spectral tensor over the wave numbers in transverse directions k_2 and k_3:

$$\chi_{ij}(k_1, \Delta_y, \Delta_z) = \\ = \int \Phi_{ij}(\boldsymbol{k}) \exp\left(i\left(k_2\Delta_y + k_3\Delta_z\right)\right) d\boldsymbol{k}_\perp \quad (5)$$

where $\int d\boldsymbol{k}_\perp = \int_{-\infty}^{\infty} dk_2 dk_3$.

The auto- and cross-correlation structure of the turbulence field in u-direction can be derived by inverse Fourier-transforming the $u-u$ cross spectrum $\chi_{11}(k_1, \Delta_y, \Delta_z)$:

$$R_{uu}(\Delta t, \Delta_y, \Delta_z) = \\ = \int_{-\infty}^{\infty} \chi_{11}(k_1\Delta_y\Delta_z) e^{ik_1\Delta t} dk_1 \quad (6)$$

The correlation quantities needed for constructing a constrained turbulence box, $\boldsymbol{\zeta}(\boldsymbol{r})$ and $\boldsymbol{Z}$, can be easily obtained by evaluating equation (6), where the distance between two points (i,j) is given as $\boldsymbol{r}_{ij} = \{|t_j - t_i|, |y_j - y_i|, |z_j - z_i|\}$, and $t_i = x_i/\bar{u}$, where $\bar{u}$ is the required average wind speed. Figure 5 plots the correlation for $\Delta t = 0$ as function of separation in y and z, with a point in the center of the y-z plane used as reference, for four different cases:

a) the theoretical values as derived from the Mann spectrum, b) an unconstrained random realization, c) a reference random realization which serves as a "target", i.e., its values are considered as constraints when constructing a constrained realization, and d) a constrained realization constructed by using the unconstrained realization b) as a basis, and selecting constraints from realization c).

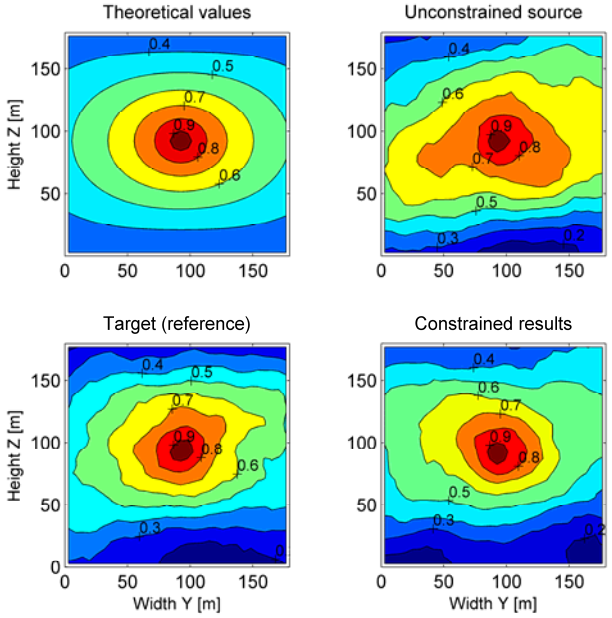

Figure 5: Contour plots of the cross-correlation in a $y-z$ plane at $\Delta t = 0$ in four different cases, based on the Mann spectral model with parameters $\Gamma = 3.9$ and $L = 72m$.

Due to the randomness of the generated wind fields and the finite length of the turbulence boxes, the observed correlations from the generated turbulence boxes plotted on Figure 5 do not match the theoretical correlation exactly. However, the correlation pattern in the constrained field bears similarities with the correlation pattern from the "reference' field, which implies that the amount of constraints applied is sufficient to increase the correlation between the constrained field and the reference field. At the locations in the y-z plane where the constraints are applied, the constrained field follows closely the behavior of the target field in the low-frequency variations (Figure 6), and matches the autocorrelation of the target field (Figure 7). The close resemblance is present at points close to the constraint locations; however for locations far away from constraints, the constrained field is still correlated with the unconstrained source field.

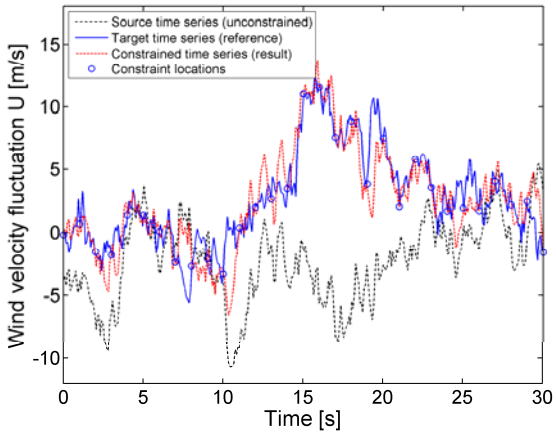

Figure 6: Comparison of constrained and unconstrained time series at a point location where a constraint is applied once per second. Constraint values are shown as blue circles.

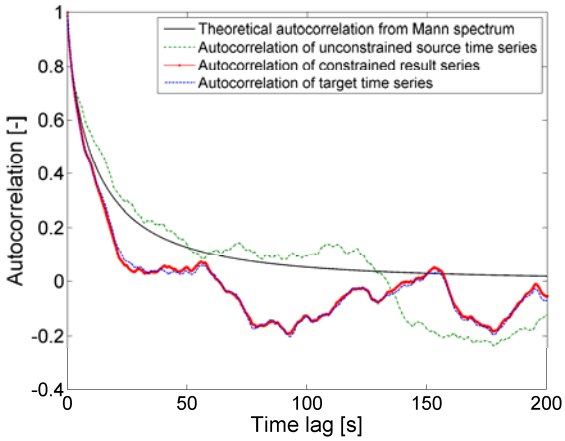

Figure 7: Comparison of autocorrelation functions at a point in the x-y plane where a constraint is applied once per second.

3. CONSTRAINED TURBULENCE FIELD AND LOAD UNCERTAINTY

In the previous section we demonstrated a method for constructing constrained turbulence fields, and showed how this method can be used to incorporate lidar measurement data in the turbulence boxes used for wind turbine load simulations. In the following, we present a numerical study assessing the possible effect of incorporating lidar measurement data on load uncertainty.

3.1. Load simulations

For the purpose of the study, we carry out dynamic load simulations using the aeroelastic code Hawc2 (Larsen and Hansen, 2012). The wind turbine used as an example is the DTU 10MW reference wind turbine (Bak et al., 2013) with rotor diameter of 179m and hub height of 119m. The simulation conditions are based on the normal production load case DLC1.1 and external conditions class IEC 1A as defined by the IEC61400-1, ed.3 standard (2005). For each study case we carry out 18 simulations per wind speed, for wind speeds between 4 and 25 m/s in 1m/s steps, resulting in 396 simulations in a study case. Each simulation in a study case uses a unique turbulence field defined by specifying different start seed number for the computer's random number generator. We make use of two sets of turbulence seeds, which we denote as $\boldsymbol{A} = [a_1, a_2, \dots, a_{396}]$ and $\boldsymbol{B} = [b_1, b_2, \dots, b_{396}]$. A total of 4 simulation sets are defined corresponding to 4 study cases:

1) A "target" reference case with simulations using unconstrained turbulence boxes from the turbulence seed set $\boldsymbol{A}$.
2) A baseline case with simulations using unconstrained turbulence boxes from the turbulence seed set $\boldsymbol{B}$.
3) Constrained case where point values from turbulence set $\boldsymbol{A}$ are incorporated as constraints to the source turbulence box set $\boldsymbol{B}$. The constraints from set $\boldsymbol{A}$ are defined at locations corresponding to the 5-beam lidar pattern. The resulting turbulence fields are denoted as set $\boldsymbol{C}$
4) Constrained case where point values from turbulence set $\boldsymbol{A}$ are incorporated as constraints to the source turbulence box set $\boldsymbol{B}$. The constraints from set $\boldsymbol{A}$ are defined at locations corresponding to the circular-scan lidar pattern. The resulting turbulence fields are denoted as set $\boldsymbol{D}$.

The turbulence length scale can influence the properties of a constrained turbulence box because it affects the correlation length, which in terms influences the distance around a constraint location where the field is affected. In order to take this into consideration, the load simulation setup described above was used to carry out two separate sets of simulations, one using a Mann turbulence model with length scale parameter of $L = 29.4m$, and another with $L = 72m$.

3.2. Uncertainty analysis

We assess the realization-to-realization uncertainty in the load simulations by calculating the ratios between the loads observed in the reference load case (set $\boldsymbol{A}$) to the loads observed in the simulations from the remaining three cases. One ratio is calculated for each turbulence seed number, leading to uncertainty variables defined as e.g.

$$X_B(i) = \frac{M(b_i)}{M(a_i)} \qquad (7)$$

where i is the seed number. $M(.)$ can be any relevant quantity that can be calculated as function of the simulated load time series, e.g., the maximum load observed, or the damage-equivalent fatigue load, DEL. a_i and b_i are the turbulence seeds from sets $\boldsymbol{A}$ and $\boldsymbol{B}$, respectively, and X_B is a variable characterizing the uncertainty in simulations with turbulence set $\boldsymbol{B}$ with respect to the reference simulation set $\boldsymbol{A}$. The assessment of the uncertainty is then based on the statistical properties of the uncertainty variables defined above. Table 1 lists the sample standard deviations of the uncertainty variables regarding the extremes of three load channels,

Table 2 compares the uncertainty in damage-equivalent fatigue loads for the same channels, while Figure 8 shows the empirically determined probability density functions.

Table 1: Standard deviations of uncertainty variables regarding absolute extreme values observed in simulations

Channel	*L*	$Std(X_B)$	$Std(X_C)$	$Std(X_D)$
Blade F	*29.4*	*0.106*	*0.075*	*0.084*
Tower S2S	*29.4*	*0.280*	*0.258*	*0.273*
Yaw	*29.4*	*0.206*	*0.131*	*0.136*
Blade F	*72*	*0.117*	*0.081*	*0.103*
Tower S2S	*72*	*0.256*	*0.241*	*0.274*
Yaw	*72*	*0.252*	*0.132*	*0.162*

Table 2: Standard deviations of uncertainty variables regarding damage-equivalent fatigue loads observed in simulations

Channel	*L*	$Std(X_B)$	$Std(X_C)$	$Std(X_D)$
Blade F	*29.4*	*0.149*	*0.083*	*0.103*
Tower S2S	*29.4*	*0.371*	*0.350*	*0.366*
Yaw	*29.4*	*0.149*	*0.053*	*0.102*
Blade F	*72*	*0.169*	*0.082*	*0.148*
Tower S2S	*72*	*0.395*	*0.344*	*0.387*
Yaw	*72*	*0.199*	*0.055*	*0.106*

For all variables the mean values were very close to 1, therefore the mean values are not reported further. The load channels considered are 1) Blade root flapwise moment (denoted "Blade F" in the tables), 2) Tower base side-to-side moment (denoted Tower S2S), and the yaw moment at tower top (denoted Yaw).

3.3. Discussion of results

The outcomes from the load analysis indicate that applying constraints to turbulence boxes results in turbulence fields which have stronger similarities to the target fields, which in terms reduces the load uncertainty. Significant reduction in load uncertainty (reduction of the standard deviation by a factor of approximately 2) was observed for blade root flapwise bending moment and tower top torsion, while the tower base side-to-side moment is practically unaffected. This observation can be explained by the assumption that modifying the turbulence boxes by adding constraints will mostly affect loads which are governed by turbulence and by the thrust force on the rotor. Loads which are not so sensitive to turbulence conditions such as the tower side-to-side moment are less affected.

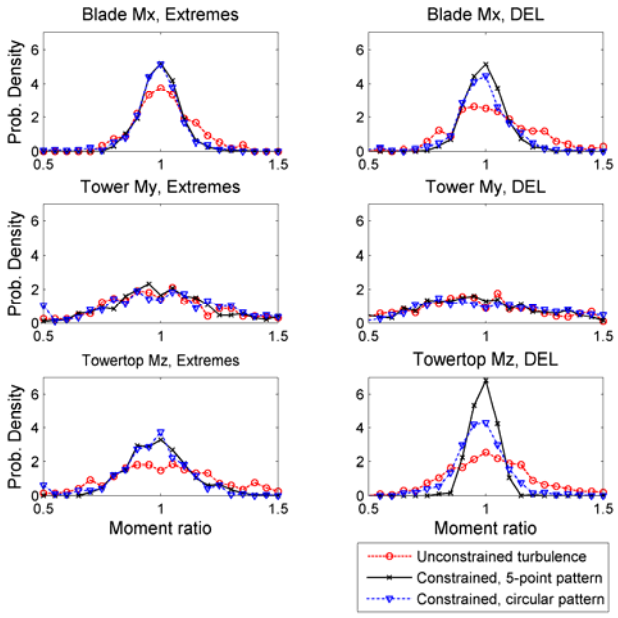

Figure 8: Observed probability densities of the ratios representing the realization-to-realization uncertainty in extreme and in damage-equivalent fatigue loads (DEL)

Another observation from the load study results is that the factor of reduction in uncertainty tends to be bigger for fatigue loads than for extremes. The overall uncertainty is slightly bigger for turbulence length scale of $L = 72$ compared to $L = 29.4$, however in the constrained cases this is compensated by a larger reduction in the uncertainty. The larger reduction in uncertainty for $L = 72$ can be explained by the larger correlation length, which results in stronger influence of the constraints on the resultant turbulence field. Furthermore, the 5-point pattern seems to perform slightly better than the circular pattern, despite being based on fewer constraints (3500 constraints per time series for the 5-point pattern vs. 8192 constraints per time series for the circular pattern). The better performance of the 5-point pattern can possibly be explained by

the presence of a central point, which results in more even distribution of the measurement points in space, having a large area covered with a coarse measurement grid. The circular pattern has more measurement points and thus finer resolution; however the fine resolution is limited to the area close to the perimeter of the circle. This indicates that the performance of the setup with a lidar scanning in a circular pattern can be improved by adding a central measurement point by e.g. another, fixed beam, or in general by designing an optimal scanning pattern better covering the area of interest.

The uncertainties estimated in the present study represent what can be considered a best-case scenario. Using purely numerical load simulations under controlled and identical conditions eliminates the majority of other uncertainties. This is an important outcome as it allows engineers to assess the efficiency of the proposed method of including lidar wind speed measurements in the turbulence field, while avoiding additional uncertainties which could mask the observed effects. When applying the same method to field measurements for loads verification purpose, it can be expected that the overall uncertainty will increase due to other contributing factors such as terrain properties, wind climate, and load measurement system.

4. CONCLUSIONS

In the present paper we demonstrated a method for incorporating wind measurements from multiple-point scanning lidars into the turbulence fields serving as input to wind turbine load simulations. A numerical study showed the application of the constrained turbulence method to load simulations on a 10MW wind turbine model, using two example lidar patterns. The results from the load calculation study showed that including lidar measurements as constraints in the turbulence field can potentially reduce the statistical uncertainty in the loads. This reduction in uncertainty can be expected for load components which are typically affected by turbulence such as blade flapwise moments, tower for-aft moment, yaw moment, and other. The turbulence length scale was shown to have an influence on the uncertainty, with larger length scales leading to larger reductions in uncertainty due to increased correlation length. Finally, the 5-beam lidar pattern was found to be slightly better performing than the circular pattern, which suggests that having the measurement points evenly distributed over a large area can be a more optimal solution than having more measurements but confined to a smaller area.

ACKNOWLEDGEMENTS

The work presented herein is a part of the Danish Innovation Fund (Innovationsfonden) project titled “UniTTe - Unified testing procedures for wind turbines through inflow characterisation using nacelle lidars”, Grant No. 1305-00024A. The financial support is greatly appreciated.

REFERENCES

Veers, P. S. (1988) “*Three-dimensional wind simulation*” Sandia National Laboratories Report No. SAND88-0152, Albuquerque, New Mexico.

Mann, J. (1994) “The spatial structure of neutral atmospheric surface-layer turbulence” *Fluid Mechanics*, 273, 141-168

Hoffmann, Y. and Ribak, E. (1991) “Constrained realizations of Gaussian fields: a simple algorithm”, *The Astrophysical Journal*, 380, L1-L8

Nielsen M., Larsen, G. C., Mann, J., Ott, S., Hansen, K. S., Pedersen, B. J. (2004) “*Wind Simulation for Extreme and Fatigue Loads*.” Tech. Rep. Risø-R-1437(EN), Risø National Laboratory, Roskilde, Denmark

Larsen, T. J., Hansen, A. M. (2012) “*How to HAWC2, the user’s manual*.” Tech. Rep. Risø-R-1597(ver.4-3) (EN), DTU Wind Energy, Roskilde, Denmark

Bak, C., Zahle, F., Bitsche, R., Kim, T., Yde, A., Henriksen, L.C., Natarajan, A., Hansen, M. (2013) “*Description of the DTU 10 MW reference wind turbine*”, DTU Wind Energy Report-I-0092

IEC. (2005) “*International Standard IEC 61400-1: Wind Turbines – Part 1: Design Guidelines*”